Temperature Sensing by Using Film Bulk Acoustic Resonator at 2.4 GHz Band

2009 Jpn. J. Appl. Phys. 48 115501

(http://iopscience.iop.org/1347-4065/48/11R/115501)

Temperature Sensing by Using Film Bulk Acoustic Resonator at 2.4 GHz Band

Yao-Huang Kao* and Jon-Hong Lin[1]

Department of Communication Engineering, Chung Hua University, Hsinchu 300, Taiwan
[1]*Department of Communication Engineering, National Chiao Tung University, Hsinchu 300, Taiwan*

Received October 12, 2008; accepted July 21, 2009; published online November 20, 2009

A four-layered film bulk acoustic resonator (FBAR) with an Al/AlN/SiN/Au composite structure was fabricated. The FBAR is composed of a surface micromachined cantilever whose copper scarification layer is released by wet etching. A temperature coefficient (TC) of resonant frequency of −34.5 ppm/°C in the temperature range from 10 to 80 °C at 2.4 GHz is obtained. Using this resonator, an oscillator for temperature sensing was constructed, in which temperature can be detected easily by measuring the shift in oscillation frequency. The TC of the oscillator is almost the same as that of the resonator.

DOI: 10.1143/JJAP.48.115501

1. Introduction

Acoustic wave devices have been widely used in various commercial applications; among these devices, surface acoustic wave resonators (SAWR) and film bulk acoustic resonators (FBAR) have shown increased use in personal communication. Sensing devices are also increasingly used because of their higher sensitivity and reliability than other related devices. Mass sensors, temperature sensors, gas sensors, chemical sensors, humidity sensors, pressure sensors, and biosensors utilizing acoustic wave devices have been reported.[1–6] Here, the focus is on temperature sensing by using FBARs.

Basically, a suspended FBAR device is a three-layer structure with the top and bottom electrodes sandwiching a middle layer of oriented piezoelectric material. Air interfaces are used on both outer surfaces to prevent acoustic energy leakage from the device; because the solid membrane and air boundary form a high impedance to acoustic waves, they function as high-Q acoustic reflectors at all frequencies. When RF signals are applied near the mechanical resonant frequency, the piezoelectric transducer excites fundamental bulk compress waves traveling perpendicular to films. Resonators used in stable oscillators should have a low temperature coefficient (TC), which needs composite structures for positive and negative coefficient compensations. However, for temperature sensing, a higher TC is required for better sensitivity, which is also achieved with the use of a composite structure containing all positive (or negative) coefficient materials.

Here, AlN is employed for potential integration. AlN has a crystal structure of hexagonal wurtzite where aluminum and nitrogen atoms are combined. An AlN film is grown along the (002) direction to achieve a strong piezoelectric coupling to the required extensional mode. An AlN lattice extends and retracts toward the c-axis orientation, inducing vibration if an alternating field is applied across the crystal.

2. FBAR Design and Fabrication

It was reported that the lower the full width at half maximum (FWHM) of a piezoelectric material, the better the performance characteristics of resonators and filters.[7] Thus, an AlN piezoelectric film should have a highly c-axis-oriented columnar structure.[8] To achieve this requirement, a SiN thin film is added between an AlN layer and a bottom electrode.[9] The SiN layer also serves as an etching stop layer to protect the bottom electrode, while patterning the AlN layer.

Table I. Physical properties of representative materials for FBAR.[10–12]

	Layer			
	Metal	Piezoelectric	Buffer	Metal
Layer material	Al	AlN	SiN	Cr/Au
Density (kg/m^3)	2700	3255	3270	19700
Acoustic velocity (m/s)	6420	10400	11000	3240 (Au)
Designed thickness (Å)	3500	11000	1000	1000
Thermal expansion coefficient (ppm/°C)	23.6	4.6	0.8	14.4

The resonant frequency of FBAR is predominantly determined by the half wavelength of a standing acoustic wave in the resonator. The fundamental resonant frequency of FBAR is then inversely proportional to the thickness (d) of the piezoelectric material used, and is equal to $V_a/2d$, where V_a is the acoustic velocity at the resonant frequency. The Nth harmonic frequency of the FBAR can be approximated as

$$f_r \approx \frac{N}{2\left(\frac{d_{elec\_t}}{V_{elec\_t}} + \frac{d_{piezo}}{V_{piezo}} + \frac{d_{SiN}}{V_{SiN}} + \frac{d_{elec\_b}}{V_{elec\_b}}\right)}, \quad (1)$$

where d_{elec_t}, d_{piezo}, d_{SiN}, and d_{elec_b} are the thicknesses of the top electrode (Al), piezoelectric material (AlN), buffer layer (SiN), and bottom electrodes (Cr/Au), respectively. V_{elec_t}, V_{piezo}, V_{SiN}, and V_{elec_b} are the acoustic velocities of the top electrode (Al), piezoelectric material (AlN), buffer layer (SiN), and bottom electrodes (Cr/Au), respectively. According to eq. (1), the thicknesses of all the layers in the FBAR for unlicensed application were designed for fundamental frequency ($N = 1$) at 2.48 GHz and are listed in Table I.

It is well known that AlN films must be oriented in the (002) direction to achieve a strong piezoelectric coupling to the required extensional mode. Therefore, columnar AlN grains whose c-axes are perpendicular to the substrate are needed. The four-layered composite structure Al/AlN/SiN/Au of FBAR is shown in Fig. 1. An AlN layer was fabricated on (100) crystallographic oriented epitaxial silicon wafers. After RCA cleaning, a silicon wafer was deposited with low-stress silicon nitride (Si_3N_4) using low-

*E-mail address: yhkao@chu.edu.tw

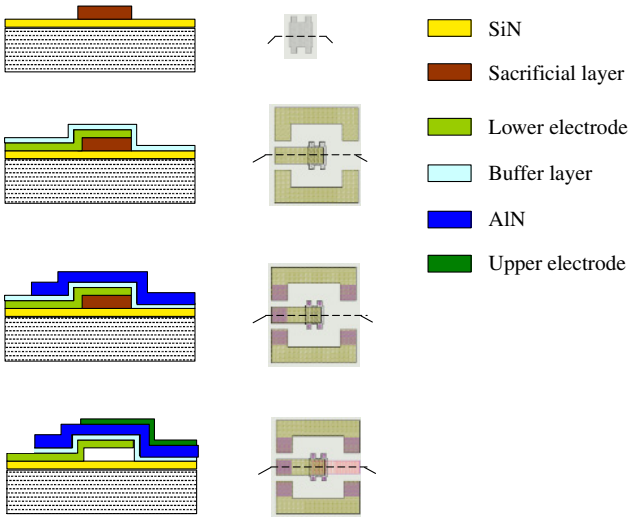

Fig. 1. (Color online) Process flow of FBAR.

pressure chemical vapor deposition (LPCVD) at a thickness of 1200 Å. The Si_3N_4 layer served both as a high-resistivity substrate to eliminate any parasitic contributions from mobile charges and as a highly boron-doped epitaxial layer to be an etch obstruction layer. A temporary support (sacrificial layer: Cu) is formed by an E-gun on top of Si_3N_4 followed by an electrode and a piezoelectric layer. Then, a thin Cr/Au film with a thickness of 1000 Å was fabricated by electron beam evaporation and patterned using a lift-off process; the film serves as the bottom electrode. The AlN film deposited on the bottom electrode had poor *c*-axis crystallinity. To solve this problem with the bottom electrode, a SiN buffer layer was introduced prior to the deposition of the bottom electrode. An amorphous SiN film with a thickness of 1000 Å was fabricated by plasma-enhanced chemical vapor deposition (PECVD), which served as a buffer layer between the bottom electrode and the piezoelectric layer.[9] An AlN film was then fabricated on top of the buffer layer by pulsed reactor DC magnetron sputtering and the substrate temperature was kept at 300 °C. The thickness of the AlN film was about 11000 Å. The fourth layer of aluminum film with a thickness of 3500 Å was fabricated by electron beam evaporation and patterned by photolithography as a top electrode. The active area of FBAR was only about $70 \times 70\,\mu m^2$ to reduce the parasitic capacitance from the electrodes for high-frequency operation. The copper temporary support with a thickness of 5000 Å was removed by wet etching using ASP100, leaving a membrane resonator supported at the edges. The die photo is shown in Fig. 2.

3. Resonator Measurement

Figures 3(a) and 3(b) show cross-sectional scanning electron microscopy (SEM) photographs of the (002)-oriented AlN film on the SiN buffer layer and the bottom electrode respectively. The cross-sectional view of the thin film shows an AlN film with a highly aligned columnar structure. The sharp boundaries of the interface between the SiN layer and the AlN film have a smooth surface.

The FBAR sensors were probed at the wafer level to measure their resonant behavior. The Agilent 8510C vector

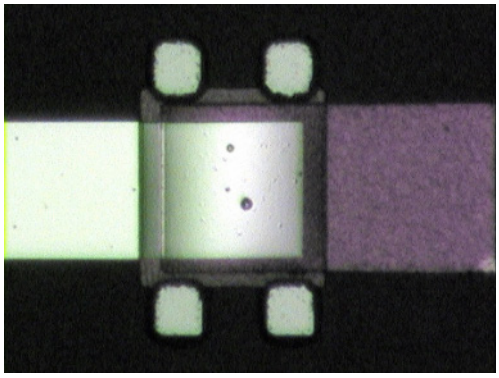

Fig. 2. (Color online) FBAR die photograph.

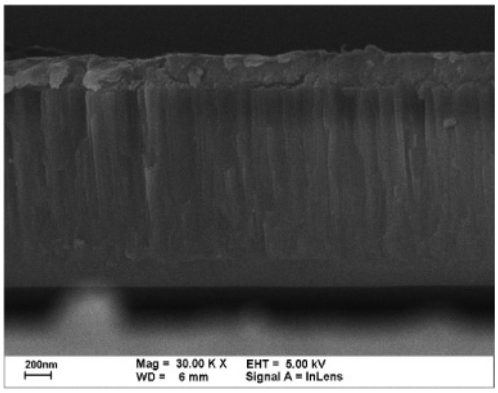

(a)

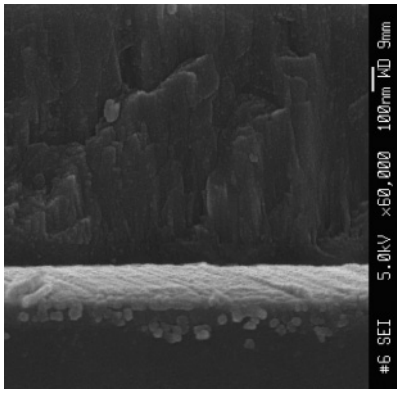

(b)

Fig. 3. Cross-sectional SEM photographs of (002)-oriented AlN film with SiN buffer layer: (a) 30000× and (b) 60000×.

network analyzer, controlled automatically by a software program, was employed to acquire the *S*-parameters. Figure 4 shows the *Z*-parameter impedance characteristics calculated from the measured *S*-parameters. The resonator reveals two resonant frequencies characterized by a zero phase shift. One is a series resonance frequency (denoted f_S) with a minimum impedance and a zero phase shift, which occurs because the piezoelectric coupling is in phase with the applied voltage. The other is a parallel resonance frequency (denoted f_P) with a maximum impedance and a zero phase shift, which occurs because the piezoelectric coupling is 180° out of phase with the applied voltage.

Temperature coefficients were determined in an open-air chamber with a temperature variation from 10 to 80 °C,

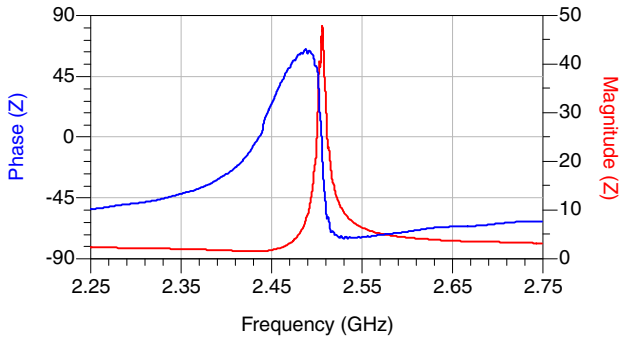

Fig. 4. (Color online) *Z*-parameters of the FBAR.

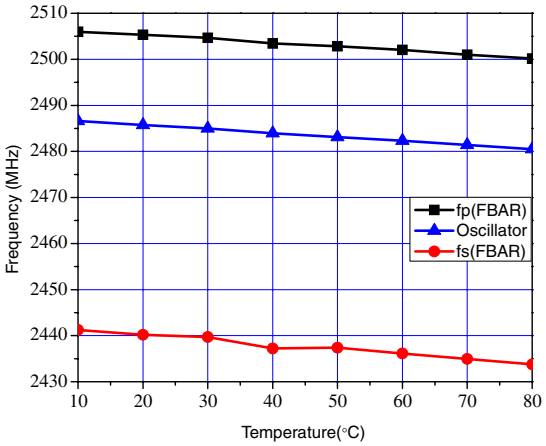

Fig. 5. (Color online) Measured variations in fundamental resonant frequency with temperature for FBAR and oscillator.

achieved by placing a heating stage on the probe station. To accurately determine the temperature at the die site, the thermal loading of the die by the probes is minimized. The measured f_S and f_P as functions of temperature are shown in Fig. 5. The TC is about $-34.5\,\mathrm{ppm/^\circ C}$ in the temperature range from 10 to 80 °C.

To verify the TC, some calculations according to eq. (1) were made. The TC for AlN is about $-25\,\mathrm{ppm/^\circ C}$.[6] The thermal expansion of AlN is about $4.6\,\mathrm{ppm/^\circ C}$.[12] We can calculate the acoustic velocity variation with temperature for AlN to be about $-29.6\,\mathrm{ppm/^\circ C}$ using the method described in U.S. patent 6452310.[13] Because of the thicknesses of the buffer layer and bottom electrode being much smaller than those of the top electrode and piezoelectric layer, we ignore their effects on the TC of FBAR. With the data listed above, we can calculate the acoustic velocity variation with the temperature for aluminum to be about $-37\,\mathrm{ppm/^\circ C}$.

4. Oscillator with Film Bulk Acoustic Resonator

With the successful realization of FBAR, an oscillator was designed and fabricated. Its functional block is illustrated in Fig. 6. The architecture of FBAR forms a feedback loop. It consists of a single loop amplifier, a Wilkinson power splitter, a phase adjustment system, and a FBAR resonator. The HBT monolithic amplifier is selected as the loop amplifier because of its low noise figure and high dynamic range. The P1dB is at +17 dBm and the bandwidth is 4 GHz. The bandwidth is properly selected to prevent high second harmonics. The nominal gain of 17 dB is much

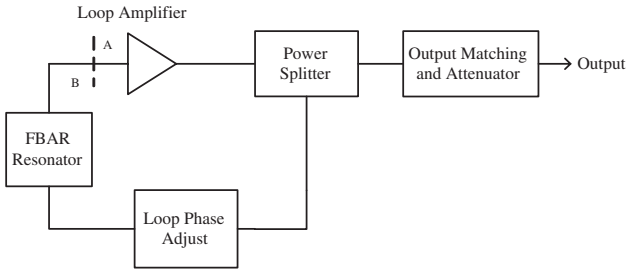

Fig. 6. Block diagram of the feedback loop oscillator.

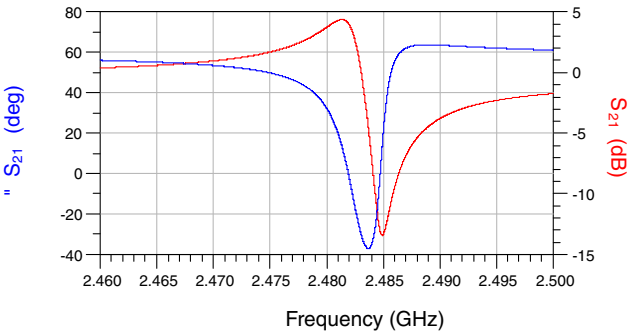

Fig. 7. (Color online) Linear simulation results for oscillator.

greater than that required to overcome the total loop losses for ensuring stable oscillation. The magnitude of gain variation over temperature is approximately $0.005\,\mathrm{dB/^\circ C}$ and this feature can prevent the temperature variation of the oscillator. The power divider and phase adjustment system are made of lumped elements. The resonator acts as a short circuit with zero phase shift at the desired frequency. The oscillation occurs as the closed loop gain satisfies Barkausen criteria.[14] During the design phase, the open loop gain (S_{21}) is actually evaluated by breaking the loop at the appropriate plane with equal input and output impedances, as shown by line AB in Fig. 6. The linear simulation is performed using agilent advance design system (ADS) software and the result is shown in Fig. 7. The oscillation starts when the phase of S_{21} is equal to zero and the magnitude S_{21} is greater than one, which in turn implies that the equivalent resistance is negative. The Barkhausen criteria are satisfied simultaneously.

The fundamental and higher harmonic oscillation spectrums were measured and are shown in Figs. 8(a) and 8(b), respectively. The second harmonics of oscillation frequency is much smaller than the fundamental resonant frequency, which improves the accuracy for the fundamental oscillation frequency measurement using a counter. The oscillation frequency is slightly higher than the series resonance frequency f_S of FBAR because of the parasitic capacitance from the package effect. The variation in fundamental frequency with temperature was also measured and is shown in Fig. 5. The TC of the oscillator is about $-34.5\,\mathrm{ppm/^\circ C}$ and seems to be equal to that of FBAR. This implies that the effective tank of the oscillator is dominated by the FBAR resonator. The oven used for long-term stability measurement requires 30 min to stabilize its inside temperature. The measurement results of the long-term stability of the FBAR oscillator are shown in Fig. 9.

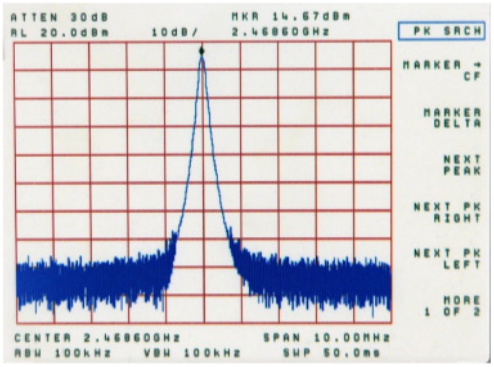

(a)

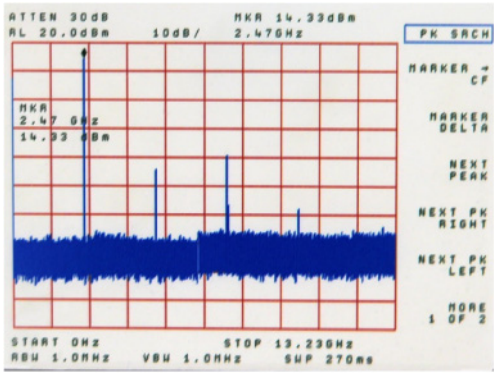

(b)

Fig. 8. (Color online) (a) Fundamental and (b) harmonic spectrums of oscillator.

5. Conclusions

A film bulk acoustic resonator for temperature sensing was designed and fabricated. Using this resonator, an oscillator operating at the 2.4 GHz unlicensed band was successfully fabricated. The fabricated and characterized temperature sensor has a sensitivity of -34.5 ppm/°C in the temperature range from 10 to 80 °C. We can easily sense the temperature variation using only a frequency counter and a FBAR oscillator.

Acknowledgements

This work is supported by Chung Shan Institute of Science and Technology (CSIST) under contract BV95G11P-001P00. The authors would like to thank Dr. P. Y. Chen and Dr. Y. C. Chin of CSIST for fabricating the samples.

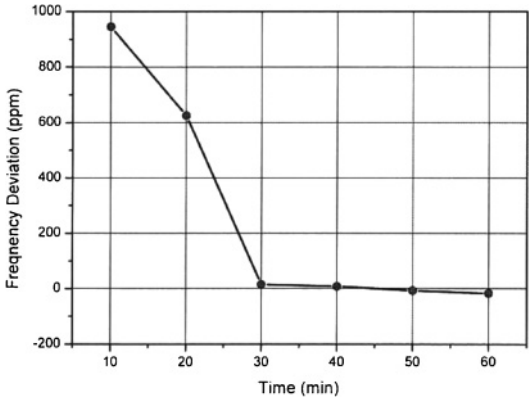

Fig. 9. Long-term stability of FBAR oscillator.

1) K. H. Chiu, H. R. Chen, and R. S. Huang: Jpn. J. Appl. Phys. **46** (2007) 1392.
2) H. Scherr, G. Scholl, F. Seifert, and R. Weigel: Proc. IEEE Ultrasonics Symp., 1996, p. 347.
3) R. Gabl, E. Green, M. Schreiter, H. D. Feucht, H. Zeininger, R. Primig, D. Pitzer, G. Eckstein, and W. Wersing: Proc. IEEE Sensors, 2003, p. 1184.
4) B. Jakoby, H. Eisenschmid, and F. Herrmann: IEEE Sens. J. **2** (2002) 443.
5) W. J. Fleming: IEEE Sens. J. **1** (2001) 296.
6) K. M. Lakin: IEEE Frequency Control Symp., 2003, We1A-4.
7) R. S. Naik, J. J. Lutsky, R. Reif, C. G. Sodini, A. Becker, L. Fetter, H. Huggins, R. Miller, J. Pastalan, G. Rittenhouse, and Y. H. Wong: IEEE Trans. Ultrason. Ferroelectr. Freq. Control **47** (2000) 292.
8) H. Lee, J. Park, K. Lee, Y. Ko, and J. Bu: Integrated Ferroelectr. **69** (2005) 323.
9) R. Aigner, L. Elbrecht, T. R. Herzog, H. Siegertsbrunn, S. Marksteiner, and W. Nessler: U.S. Patent 6878604B2 (2005).
10) G. S. Kino: *Acoustic Waves: Devices, Imaging, and Analog Signal Processing* (Prentice Hall, Upper Saddle River, NJ, 1987) p. 549.
11) W. Pang, H. Yu, H. Zhang, and E. S. Kim: IEEE Electron Device Lett. **26** (2005) 369.
12) G. F. Iriarite: Dr. Thesis, Faculty of Science and Technology, Uppsala University, Sweden (2003).
13) C. M. Panasik: U.S. Patent 6452310 (2002).
14) G. D. Vendelin, A. M. Pavio, and U. L. Rohde: *Microwave Circuit Design Using Linear and Nonlinear Techniques* (Wiley, Hoboken, NJ, 2005) 2nd ed., p. 550.